Eur. Phys. J. A (2018) **54**: 205
DOI 10.1140/epja/i2018-12634-y

THE EUROPEAN PHYSICAL JOURNAL A

Regular Article – Experimental Physics

Analysis of experimental cross-section for (α, n) reactions in odd A and odd Z heavy nuclei: A systematics on pre-compound emission

Manoj Kumar Sharma[1,a], Mahesh Kumar[1], Mohd. Shuaib[2], Vijay R. Sharma[3], Abhishek Yadav[4], Pushpendra P. Singh[5], Devendra P. Singh[6], B.P. Singh[2], and R. Prasad[2]

[1] Department of Physics, Shri Varshney College, Aligarh-202 001, India
[2] Accelerator Laboratory, Physics Department, Aligarh Muslim University, Aligarh-202 002, India
[3] Departamento de Aceleradores, Instituto Nacional de Investigaciones Nucleares, Apartado Postal 18-1027, C.P. 11801 Ciudad de Mexico, Mexico
[4] NP-Group, Inter-University Accelerator Centre, New Delhi-110 067, India
[5] Department of Physics, Indian Institute of Technology Roopnagar, Ropar-140 001, India
[6] Department of Physics, University of Petroleum and Energy Studies, Dehradun, India

Received: 3 August 2018 / Revised: 25 September 2018
Published online: 30 November 2018

Communicated by P. Rossi

Abstract. Aiming to develop a systematics in the pre-compound emission process and to get its driving parameters, a sensitive analysis of the measured excitation functions for (α, n) reaction channel on target nuclei viz., ^{139}La, ^{159}Tb, ^{181}Ta, ^{197}Au and ^{203}Tl has been performed with codes PACE4 and ALICE at low projectile energies, where the compound nucleus process is dominant. The code PACE4 considers only compound nucleus emission, while the ALICE code takes into account both compound and pre-compound emissions. The observed enhancement in experimental excitation functions in the tail portion of energies as compared to calculations performed with code PACE4 may be attributed to the contribution from pre-compound emission. Further, the calculations performed with the ALICE code confirm the significant contribution of the pre-compound emission. The effect of various pre-compound parameters on measured excitation functions has also been studied. The energy dependent yield of the pre-compound contribution over the compound nucleus emission for neutron emission channels is deduced in terms of pre-compound fraction "F_{PCN}" which gives a good systematics on such process. The developed systematics in α-induced reactions on target nuclei reflects that the pre-compound process is governed by the excitation energy available with the nucleons at the surface of the composite systems. Furthermore, the mass number of the target nuclei may also play an important role in the pre-compound process at low projectile energies.

1 Introduction

During the past few decades, the mechanism of pre-compound (PCN) emission has been a topic of fundamental interest in α-particle induced reactions at low and intermediate energies. Earlier many of the theoretical and experimental studies have triggered the observation of such phenomenon at relatively higher energies. Recent studies showing the observations of PCN emission even at low incident energies where evaporation process dominates, have renewed interest to carry out further research in the aforesaid reaction mechanism [1–5]. The term PCN mechanism refers to the process in which the emission of particle takes place at any stage during gradual redistribution of incoming particle's energy among more and more nuclear degree of freedom through a chain of particle-hole excitations well before to the establishment of statistical equilibrium [6–8]. The emitted particles in this process are known as pre-compound or pre-equilibrium particles. On the other hand, the process in which particle emission occurring through evaporation after statistical equilibrium has been achieved is referred to either as compound nucleus (CN) emission process or as evaporation process. Hence, the key role of PCN emission in the reaction mechanism is that it reflects the dynamics of decay of an excited composite system through different quasi-equilibrated states leading to the formation of a compound nucleus.

Understanding the PCN reaction mechanism is one of the most challenging problems in nuclear reaction physics

[a] e-mail: manojamu76@gmail.com

as there is no sharp boundary between the above two processes. Some times direct reactions, which are the ones involving a single target-projectile interaction may also mix with PCN emission contributing to make the data analysis more complex, although, there are many other complexities in PCN processes. Despite the overall complexity of the PCN process, one can study these processes experimentally using different techniques and looking to different physical quantities, through the following measurements viz., i) estimating the difference in the flux of emitted particles in the forward direction over the backward direction, ii) measuring particle (n, p and α) spectra in the time-of-flight experiments in coincidence with γ-rays characteristic of specific reaction residues [9], iii) detecting deviations from CN formation and decay in terms of PCN process through γ-ray multiplicity measurements [10,11], iv) measuring the recoil energy/velocity of residual particles left after particle emission, v) measuring the angular distribution of emitted light particles, vi) comparing the measured excitation functions (EFs) with theoretical predictions. These measurements help in characterizing the PCN emission process.

Some of the important experimental characteristics of the PCN emission over the CN process are i) the presence of a larger number of high-energy particles as compared to the spectrum predicted by the statistical model (CN) [12], ii) forward-peaked angular distribution of the emitted particles [13], iii) observations of relatively smaller recoil range/linear momentum of the reaction residues left over the emission of PCN particles as compared to CN particles [14], iv) observations of lower values of the spin for the PCN process as compared to the CN process [14], v) slowly decreasing tails of the EFs [1,2,5,15], etc.

Furthermore, the measurement and analysis of the EFs are of primary interest because the features of the EFs at the low, medium and high energies may give a direct indication of the reaction mechanism involved [16–20]. The low energy portion of the EFs is dominated by the CN mechanism, however, with the increase in projectile energy, the strength of the PCN processes becomes relatively larger [1,2,8,21–26]. Recently several authors [6,27–34] have reported the data on α-induced reactions for the study of the pre-compound emission process. Mohr [28] performed the analysis of excitation functions for several α-induced reactions over a wide range of projectile energies for a broad mass region by introducing a simple reduction scheme based on reduced energy E_{red} and reduced cross-sections σ_{red}. Yigit and Korkmarz [29] have measured the excitation functions of several reactions in the fusion of α and proton beams with heavy target nuclei ^{181}Ta. They have reported that pre-compound neutrons are subsequently emitted during the thermalization of the excited composite system. Suchiang *et al.* [30] have also performed the analysis of measured excitation functions by using a set of global parameters of code TALYS with a view to study the pre-compound emission occurring in the interaction of α beam with ^{181}Ta target at energy ranging from $\approx$ 20 to 80 MeV. Mohan Rao and Chintalapudi [31] have carried out the measurements and analysis of the excitation functions for alpha particle induced reactions on the targets ^{169}Tm and ^{181} Ta up to 60 MeV using the stacked foil activation technique. The above studies suggest that the pre-compound reaction mechanism is one of the dominant reaction processes in alpha-particle induced reactions. Though, a large amount of data on the PCN emission is available in the literature, but not enough and complete systematics are available on this complex process.

With this motivation, we performed a systematic, unified and consistent analysis of EFs for reactions ^{139}La$(\alpha,n)^{142}$Pr [35], ^{159}Tb$(\alpha,n)^{162}$Ho [36], ^{181}Ta$(\alpha,n)^{184}$Re [37,38], ^{197}Au$(\alpha,n)^{200}$Tl [39], and ^{203}Tl$(\alpha,n)^{206}$Bi [40], respectively. It may be pointed out here that EFs for reaction ^{179}Au$(\alpha,n)^{182}$Tl has been measured earlier by our group by using the stacked foil activation technique, while the cross-section data of other reactions has been taken from the EXFOR data library [41]. The analysis of these EFs has been performed by comparing experimental data with simulations performed using both the PACE [42] and ALICE [43] codes. The code PACE [42] is a statistical model which describes the decay by an excited compound nucleus and calculates the fusion cross-section based on the Bass model [44], while the ALICE [43] code is a composite code which takes into account of both pre-equilibrium and equilibrium phases. The CN calculations in the ALICE code are performed using the Weisskopf-Ewing model [45], while the PCN component is simulated using the Geometry Dependent Hybrid model [46]. The work underlying this paper has been performed as part of our ongoing program of measurements and analyses of cross-section data in light and heavy ion induced reactions. The present work is an attempt to get a systematics of PCN emission at low projectile energies in α-induced reactions, where the probability of the emission of single neutron through the PCN process is quite greater as compared to the reactions leading to the emission of more than one particle through xn, xpn channels etc. To the best of our knowledge no such attempt has been made to develop systematics for PCN process so far. It may be pointed out here that the target nuclei chosen for the present study have odd atomic Z and odd mass A numbers in order to wash out ambiguity, if any, arising due to the odd even effect of the targets.

This paper is organized as follows. A brief discussion on the experimental technique is given in sect. 2, while sects. 3 and 4 deal with the analysis of the EFs with codes PACE4 and ALICE, respectively. Details on the systematics on the PCN process are given in sect. 5. The conclusions drawn from the above analysis are summarized in sect. 6 of the paper.

2 Experimental technique

The activation technique was employed for the measurements of EFs for the reactions ^{139}La$(\alpha,n)^{142}$Pr [35], ^{159}Tb $(\alpha,n)^{162}$Ho [36], ^{181}Ta$(\alpha,n)^{184}$Re [37,38], ^{197}Au(α,n) ^{200}Tl [39], and ^{203}Tl$(\alpha,n)^{206}$Bi [40]. In this experimental technique, a stack consisting of several targets followed by catcher foils is irradiated in the scattering chamber for

several hours depending on the half-lives of the reaction residues and their production yield. The most important advantage of this technique is that the EFs of the production residues at several energies have been measured in a single irradiation. For the ready reference a brief discussion on the experiment performed at the Variable Energy Cyclotron Centre (VECC), Kolkata, India by the activation technique is given. A stack consisting of three pure natural gold (^{197}Au) targets was irradiated for ≈ 12 h by a collimated α-particle beam obtained from a VECC of maximum energy ≈ 40 MeV. The beam current ≈ 100 nA was monitored from the current integrator count rate. The calculations for average beam energy on a given target of the stack have been performed using the stopping power program SRIM [47]. The activities induced in the samples analysis have been carried out by using a high resolution large volume (100 c.c.) high-purity germanium (HPGe) detector coupled to a multi parameter CANBERRA system. In the present work, a ^{152}Eu point γ-source is used to determine the efficiency of the HPGe detector for various gamma energies ranging from 121 keV to 1408 keV. During the counting of the samples, the sample-detector distances are suitably adjusted in order to minimize the dead time to $< 10\%$.

The residual nuclei produced in the $\alpha + {}^{179}$Au system have been identified by their characteristic γ-rays and the measured half-life. The pertinent decay data used in the present work for the yield calculations has been taken from ref. [48]. The cross-sections for the production of the residual nuclei of interest have been determined from the observed γ-activity after proper background correction by using the standard formulations [20]. The overall experimental errors in the present measurements are expected to be $< 10\%$. A detailed discussion on experimental errors due to various factors viz., number of target nuclei, the fluctuation of beam current, detector efficiency, the dead time of the counting system, etc., is given in ref. [20].

3 Analysis of experimental EFs with code PACE4

The calculations for the measured cross-sections of the evaporation residues have been performed using code PACE4 [42], which is based on a statistical approach. The de-excitation of the compound nucleus is followed by the Monte Carlo procedure. In this code the angular momentum projections are calculated at each stage of de-excitation, which enables the determination of angular distribution of the emitted particles. The cross-sections of evaporation residues are calculated using the Bass formula [44], as given below.

For the compound nucleus formation, at a particular angular momentum ℓ and specific bombarding energy E, the partial cross-section σ_ℓ, is given by

$$\sigma_\ell = \frac{\lambda^2}{4\pi}(2\ell + 1)T_\ell, \tag{1}$$

where λ is reduced wavelength and the transmission coefficients T_ℓ may be given by the expression

$$T_\ell = \left[1 + \exp\left(\frac{\ell - \ell_{\max}}{\Delta}\right)\right]^{-1}, \tag{2}$$

where Δ is the diffuseness parameter, while $\ell_{\max}$ is the maximum value of ℓ determined by total fusion cross-section,

$$\sigma_F = \sum_{\ell=0}^{\infty} \sigma_\ell. \tag{3}$$

The optical model parameters for neutron, proton and α-emission were taken by using the default option of code PACE4 [42]. The γ-ray strength functions for $E1$, $E2$ and $M1$ transition were taken from tables of Endt [49]. The present version of code uses the excitation energy dependent level density parameter using the prescription of Kataria *et al.* [50]. The level density used in this code is calculated from the expression $a = (A/K)$, where, A is the mass number of the compound nucleus and K is a free parameter known as the level density parameter constant. In the present work, a value of $K = 8$ is taken in the calculations, which is widely accepted. The experimentally measured and theoretically calculated EFs for reactions ^{139}La$(\alpha, n)^{142}$Pr and ^{159}Tb$(\alpha, n)^{162}$Ho are shown in figs. 1(a) and (b), while for reactions ^{181}Ta$(\alpha, n)^{184}$Re, ^{197}Au$(\alpha, n)^{200}$Tl, and ^{203}Tl$(\alpha, n)^{206}$Bi are shown in fig. 2(a)–(c), respectively. The dashed curves in these figures represent the best fitted experimental data guide to the eye, while solid curves represent calculations of the code PACE4. It may be pointed out that in the literature [37,38], the meta stable and ground states of ^{184}Re are measured separately. As such, the cross-section for the sum of both these states has been compared with model calculations. As can be seen from these figures (fig. 1(c) and fig. 4(c)) the theoretical calculations agree well with the experimental data up to the peak portion. In the tail portion of EFs, deviation of the experimental data as compared to PACE4 calculations has been observed. The higher values of experimental cross-sections in the tail portion of EFs for these reactions as compared to the theoretical calculations may be attributed to the PCN emission process, which is a dominant mode of mechanisms in one neutron emitting reaction channels at these energies and is not considered in the PACE4 calculations, which may be confirmed by comparing the measured EFs with the calculations done by the ALICE code and which are discussed in the next section of this paper.

4 Analysis of experimental EFs with the ALICE code

The ALICE code developed by Blann [43], has been used to calculate the cross-sections for the CN and the PCN emission processes. The CN calculations are performed by using the Weisskopf-Ewing model [45], while, the CN+PCN

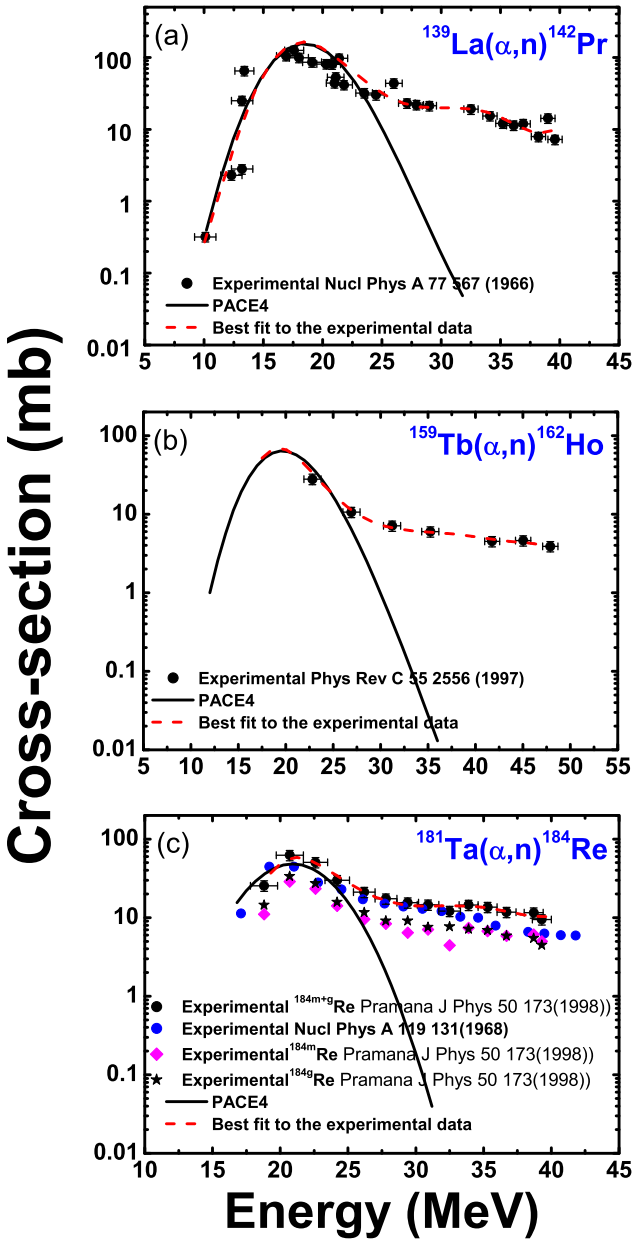

Fig. 1. (Color online) The experimental and theoretical calculated EFs for reactions ^{139}La$(\alpha,n)^{142}$Pr, ^{159}Tb$(\alpha,n)^{162}$Pr and ^{181}Ta$(\alpha,n)^{184}$Re, respectively. In these figures, the curves represent PACE4 calculations for pure compound nucleus, while the dotted curves guide to the experimental data. The details of the calculations are discussed in the text.

components are simulated by employing the Geometry Dependent Hybrid (GDH) model [46]. The emissions of neutron, proton, deuteron and/or α particles are considered in this code. The Myers-Swiatecki/Lysekil mass formula [51] is used for calculating the Q-values and the binding energies of all the nuclei in the evaporation chain. The calculations for the PCN emission in this code are performed assuming the equipartition of energy among initially excited particles and holes. The mean free path (MFP) for intranuclear transition rates may be calculated either from

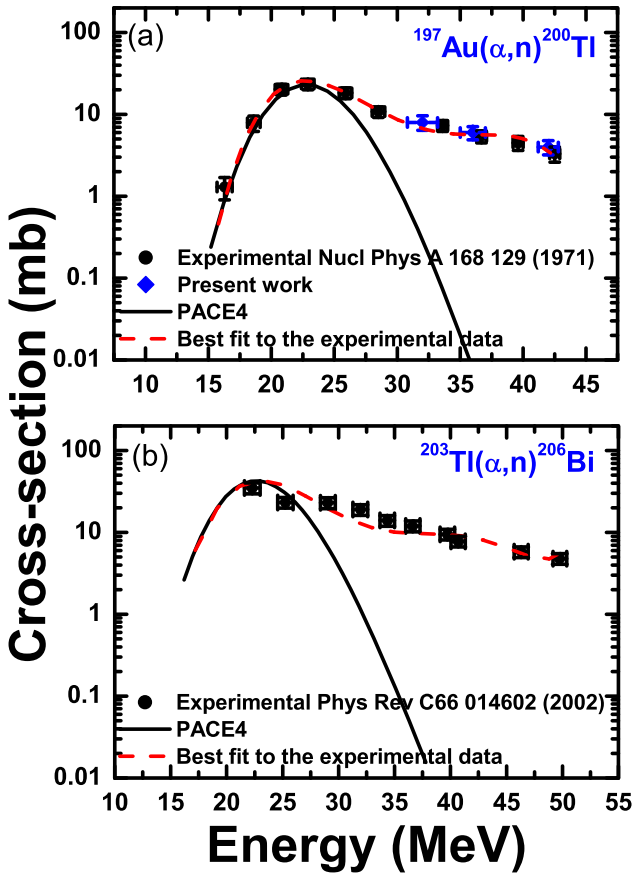

Fig. 2. (Color online) The experimental and theoretical calculated EFs for reactions ^{197}Au$(\alpha,n)^{200}$Tl and ^{203}Tl$(\alpha,n)^{206}$Bi. In these figures, the curves represent PACE4 calculations for pure compound nucleus, while the dotted curves guide to the experimental data. The details of the calculations are discussed in the text.

the optical potential parameters of Becchetti and Greenlees [52] or from Pauli corrected nucleon-nucleon cross-sections [53,54]. In the present calculations, the optical potentials of Becchetti and Greenlees [52] have been used. The differential cross-section for emitting a particle with channel energy ε may be written as (cross-section per unit energy to emit a particle of type ν)

$$\frac{\mathrm{d}\sigma}{\mathrm{d}\varepsilon}_{\nu} = \frac{\pi\lambda^2}{4\pi^2}\sum_{I=|0|}^{\infty}(2I+1)T_I(2S_\nu+1)\sum_{l=|0|}^{\infty}T^l{}_\nu(\varepsilon) \times \sum_{J=|I-l|}^{I+l}\rho(\varepsilon,J)/D, \quad (4)$$

where λ is the de-Broglie wavelength of the incident ion, T_I the transmission coefficient of the I^{th} partial wave of the incident ion, $\rho(\varepsilon,J)$ the spin dependent level density for the residual nucleus, D the integral of numerator over all particles and emission energies, and ε the excitation energy of the compound nucleus. S_ν is the intrinsic spin of the particle ν, $T^l{}_\nu(\varepsilon)$ is the transmission coefficient for the particle ν with kinetic energy ε and orbital angular momentum l.

In this code, the level density parameter a, the initial exciton number n_0, and the mean free path multiplier COST are some of the important parameters. The level density parameter a mainly affects the CN component, while the initial exciton number n_0 and the mean free path multiplier COST govern the PCN component. The physical description of these parameters and their effects on measured EFs is also important to be discussed. The nuclear level density is defined as the number of nuclear states per excitation energy interval, realized as a specific pattern of single particle excitations, at a given excitation energy. The value of level density parameter a may be calculated from the expression $a = A/K$ where, A is the mass number of the composite nucleus and K is an adjustable parameter [55]. In our earlier analysis it has been observed that the value of $K = 8$ gives best fit to the experimental data over the entire range of projectile energies for α-induced reactions [5,56]. Further, in the geometry dependent hybrid model, the intermediate states of a nuclear system are characterized by the excitation energy E^* and the number n_p of excited particles and n_h of excited holes. The particles and holes are defined relative to the ground state of the nucleus and are called excitons.

The initial configuration of the compound system defined by the exciton number $n_0 = (n_p + n_h)$ is a crucial parameter of the PCN formalism that determines the shape of EFs in the higher energy region. In order to get the value of initial exciton number n_0, the calculations for different values of n_0 ranging from 4 to 6 with configurations $(2p + 2n + 0h)$ for $n_0 = 4$, $(3p + 2n + 0h)$ for $n_0 = 5$ and $(3p + 2n + 1h)$ for $n_0 = 6$, respectively, have been performed for reaction ^{203}Tl$(\alpha, n)^{206}$Bi and are shown in fig. 3(a). It may be observed from fig. 3(a), that a value of initial exciton number $n_0 = 4$ fits the experimental data satisfactorily over the entire range of energies. A value of initial exciton number $n_0 = 4$ for α-induced reactions is justified [46]. The lower value of initial exciton number n_0 gives larger PCN contribution. It is because of the fact that the lower value of n_0 means a larger number of two-body interactions prior to the establishment of thermodynamic equilibrium, resulting in larger PCN contribution. The mean free path multiplier COST is another important parameter in the ALICE code for the PCN formalism that accounts for difference, if any, between the calculated and actual mean free paths for two body residual interactions and is used to adjust the nuclear mean free path in order to reproduce the experimental data. The effect of variation of parameter COST *i.e.*, COST = 0 and COST = 2 on the calculated EF for the reaction ^{203}Tl$(\alpha, n)^{206}$Bi is shown in fig. 3(b). As can be seen from this figure, a value of COST = 2 along with $K = 8$ and $n_0 = 4$ gives best fit to the experimental data over the entire range of projectile energies. These values of input parameters of the ALICE code are considered to reproduce the data for α-induced reactions on other target nuclei as well.

In order to get systematics in α-induced reactions on various targets having odd Z and odd A in the mass region 139 to 197, the experimental data of one neutron channel in reactions ^{139}La$(\alpha, n)^{142}$Pr [35], ^{181}Ta$(\alpha, n)^{184}$Ra [37, 38], ^{159}Tb$(\alpha, n)^{162}$Ho [36] and ^{197}Au$(\alpha, n)^{200}$Tl [39] has also been analyzed with the same set of parameters. The theoretical calculations along with experimental EFs for these reactions with $K = 8$, $n_0 = 4$ and COST = 2 are shown in fig. 4(a)–(d), respectively, with their experimental values. It may be observed that ALICE calculations with the same set of parameters satisfactorily reproduce the experimental EFs for all the presently studied systems.

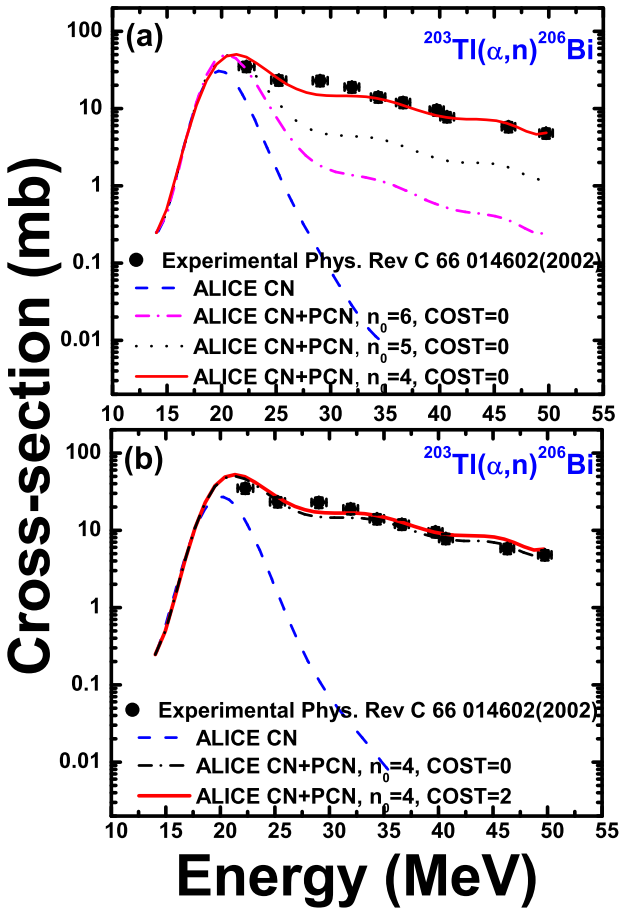

Fig. 3. (Color online) The experimental and theoretically calculated EFs for reaction ^{203}Tl$(\alpha, n)^{206}$Bi using the ALICE code. Figure 3(a) represents the effect of variation of parameter n_0 from 4 to 6 in ALICE calculations. In this figure, the dashed curve represents compound nucleus calculations obtained by the Weisskopf-Ewing model [45], while, the solid, dotted and dash dotted curves are corresponding to the values of parameter $n_0 = 4$, 5, and 6, respectively, obtained by using the Geometry Dependent Hybrid (GDH) model [46] of code ALICE to represent the CN+PCN components. Figure 3(b) represents the effect of different values of mean free multiplier COST = 0 and COST = 2.0 in ALICE on the theoretical calculations. The details of these parameters are discussed in the manuscript.

5 Systematics of the pre-compound process

In order to obtain the systematics of the PCN process, the contribution of PCN in each reaction has been deduced in the form of pre-compound fraction (F_{PCN}) that reflects the relative importance of the PCN process over

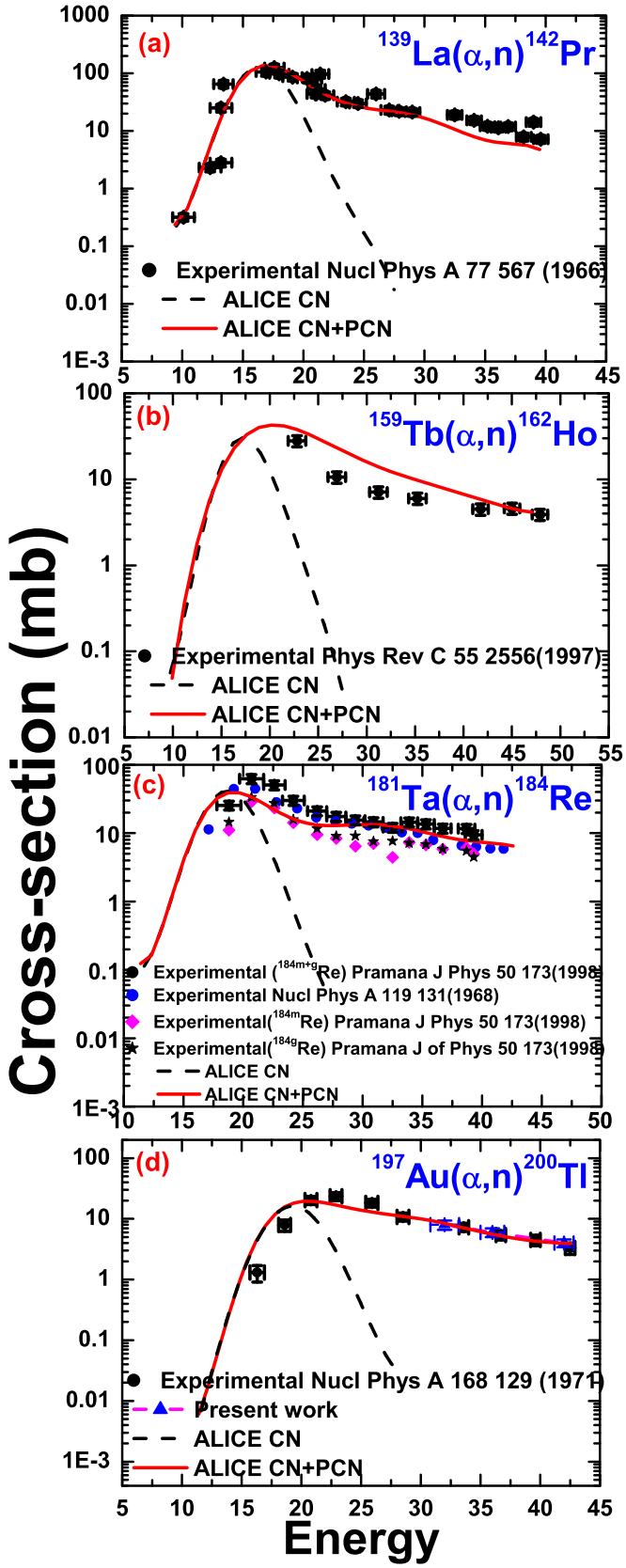

Fig. 4. (Color online) The experimental and theoretical calculated EFs for reactions ^{139}La$(\alpha,n)^{142}$Pr, ^{159}Tb$(\alpha,n)^{162}$Ho, ^{181}Ta$(\alpha,n)^{184}$Re and ^{197}Au$(\alpha,n)^{200}$Tl. The details of the calculations are discussed in the text.

the CN process. The F_{PCN} is deduced by the ratio of the difference of the cross-sections for the (PCN+CN) emission and the CN cross-sections to the cross-section values of (PCN+CN). The deduced "F_{PCN}" values in percentage are plotted as a function of the centre of mass energy E_{CM} for the reactions ^{139}La$(\alpha,n)^{142}$Pr, ^{159}Tb$(\alpha,n)^{162}$Ho, ^{181}Ta$(\alpha,n)^{184}$Re, ^{197}Au$(\alpha,n)^{200}$Tl, and ^{203}Tl$(\alpha,n)^{206}$Bi respectively and are shown in fig. 5(a). As can be seen from this figure the "F_{PCN}" for these reactions increases with the centre of mass energy "E_{CM}" for each target. The small variation in E_{CM} produces a large change in F_{PCN}. The values of E_{CM} at which "F_{PCN}" starts and attain its maximum are different for different targets. As can be seen from fig. 5(a) F_{PCN} starts increasing at a lower value of E_{CM} for lighter mass target nuclei from ^{139}La to ^{203}Tl. However, data collected for the target ^{197}Au do not follow the trend. Therefore, no clear systematic dependence on E_{CM} can be deduced for the studied systems.

Furthermore, looking for a systematic effect on the PCN of the mass number as a function of the excitation energy, the values of deduced "F_{PCN}" are plotted as a function of the excitation energy for the reactions ^{139}La$(\alpha,n)^{142}$Pr, ^{159}Tb$(\alpha,n)^{162}$Ho, ^{181}Ta$(\alpha,n)^{184}$Re, ^{197}Au$(\alpha,n)^{200}$Tl, and ^{203}Tl$(\alpha,n)^{206}$Bi and are shown in fig. 5(b). The only observation which can be deduced in this case is that the threshold value of the excitation energy at which "F_{PCN}" begins is lower for the heavier target ^{203}Tl. Beside the fact this is just opposite to the case as discussed in fig. 5(a). We can just conclude that again there is no evidence of any systematic trend of the PCN and target mass with respect to excitation energy.

As a matter of fact in the PCN emission the participation of nucleons on the surface of the composite system is more probable as compared to the nucleons well inside, as such, the excitation energy per nucleon available at the surface E_S of composite system ($E_S = E^*/A^{2/3}$) may be used as another parameter to influence the PCN process. To get a systematic trend, the "F_{PCN}" for the above systems are plotted as a function of E_S and are shown in fig. 5(c). As can be seen from this figure, a systematic trend of the "F_{PCN}" in terms of mass of the target nuclei and the excitation energy per nucleon at the surface of the composite system is observed for all the targets studied in the present work. This may give support to the indication that in the PCN emission all the nucleons of the composite system are not involved in the PCN reaction mechanism. As such, the PCN emission may have a significant effect from the surface interactions. In other words, this may indicate that particles interacting in the nuclear periphery may have a better chance to be emitted as PCN particles, where an average lower density is present, as compared to the particles passing through the entire diameter of the target and therefore underlying the effect of a higher density nuclear matter region.

In the present work, the conclusion drawn from the above study provides a new systematics for the PCN process in α induced reactions and has been shown in fig. 6. This figure shows variation of the pre-compound fraction ("F_{PCN}") with mass number of target nuclei (A) at five different values of the excitation energy per nucleon E_S

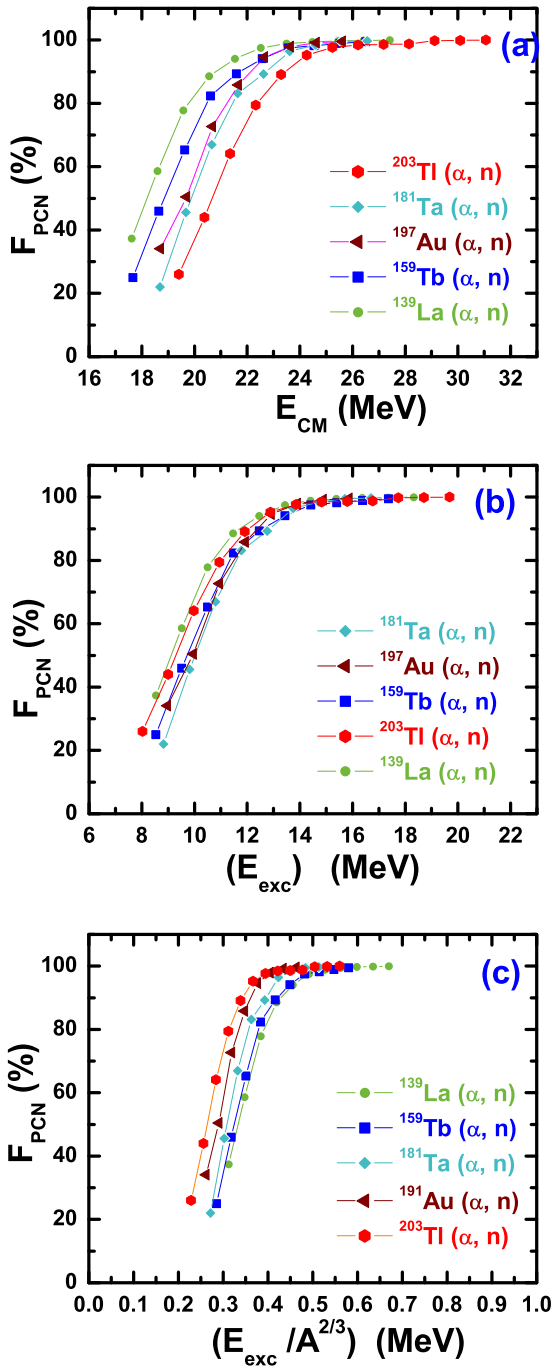

Fig. 5. (Color online) (a) The deduced F_{PCN} as a function of the centre of mass energy E_{CM} for the reactions ^{139}La$(\alpha,n)^{142}$Pr, ^{159}Tb$(\alpha,n)^{162}$Ho, ^{181}Ta$(\alpha,n)^{184}$Re, ^{197}Au $(\alpha,n)^{200}$Tl, and ^{203}Tl$(\alpha,n)^{206}$Bi. Figures (b and c) represent the dependence of F_{PCN} on the excitation energy E_{exc} and the excitation energy per surface nucleons $E^*/A^{2/3}$ for these reactions, respectively.

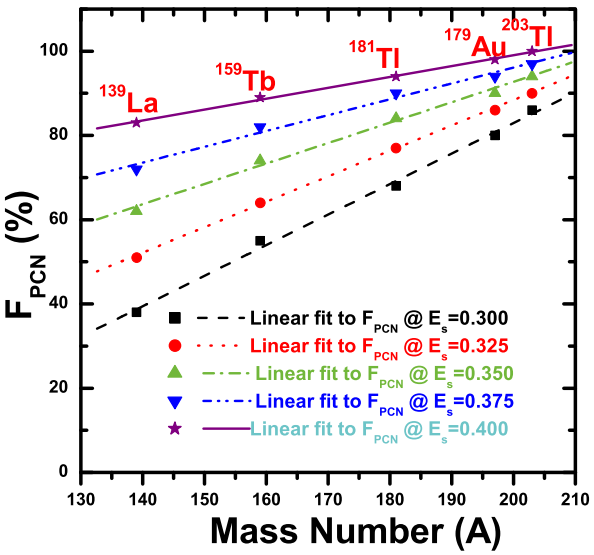

Fig. 6. (Color online) Deduced pre-compound fraction "F_{PCN}" as a function of mass number of the target nuclei. The pre-compound fraction "F_{PCN}" linearly increases with the mass of the target nuclei from $A = 139$ to $A = 203$. In this figure, deduced "F_{PCN}" presently studied targets are shown by different symbols with different lines (target ^{138}La shown by the dashed line with black solid squares, ^{159}Tb by the dotted line with red sold circles, ^{181}Ta by the dash dotted line with green up triangles, ^{179}Au by the dash–double-dotted blue line with blue down triangles and ^{203}Tl by solid purple line with purple stars).

(= 0.300, 0.325, 0.350, 0.375 and 0.400 MeV, respectively) available at the surface of composite systems. As can be seen from this figure, "F_{PCN}" increases linearly with mass number (A) of the target nuclei (in fig. 6 target ^{138}La has been shown by a dashed line with black solid squares, ^{159}Tb by a dotted line with red sold circles, ^{181}Ta by a dash-dotted line with green up triangles, ^{179}Au by a dash–double-dotted blue line with blue down triangles and ^{203}Tl by a solid purple line with purple stars) at each value of E_S for the presently studied systems.

It may be observed from fig. 6, that fitted lines for different values of E_S which guide the deduced "F_{PCN}" are not exactly parallel to each other hence, they have different values of slope. The slope of the lines decreases with increase in the excitation energy per surface nucleon E_S. It means that the probability of the PCN increases as the mass of target nuclei increases at a fixed value of E_S. At higher values of the excitation energy per surface nucleon E_S, these lines start conversing which reflects that the contribution of the PCN process saturates and becomes maximum for each target for one neutron emitting channels. Further increases in the excitation energy per surface nucleon E_S, increases the probability of two neutron emission. As such, the systematics obtained from the present analysis is interesting and allows additional insight in our understanding of the PCN emission process.

6 Conclusions

The analysis of experimental EFs on heavy target nuclei viz., ^{139}La, ^{159}Tb, ^{181}Ta, ^{197}Au and ^{203}Tl in α-induced reactions has been performed by the codes PACE4 and ALICE, respectively. The observed enhancement in the experi-

mental excitation functions for reactions ^{139}La$(\alpha, n)^{142}$Pr, ^{159}Ta$(\alpha, n)^{162}$Ho, ^{181}Ta$(\alpha, n)^{184}$Re, ^{197}Au$(\alpha, n)^{200}$Tl, and ^{203}Tl$(\alpha, n)^{206}$Bi as compared to PACE4 calculations indicates that these reactions do not independently proceed through compound nucleus process and may have significant contribution to the pre-compound emission process as well. It has to be reminded that at these energies the contribution of direct reaction is negligible. Furthermore, the calculations performed with the ALICE code have reproduced the experimental data of the measured excitation function for these reactions in the presently studied energy region, satisfactorily. It has been concluded that experimentally measured excitation functions could be reproduced only when the pre-compound emission, simulated theoretically by using the ALICE code, has been taken into account for the aforesaid reactions. It has further been observed that the same set of parameters of the ALICE code satisfactorily reproduces the experimental existing data for all the presently studied systems that have been used to develop a systematics in α-induced reactions. The systematics deduced in the presently studied mass region having odd A and odd Z value of target nuclei indicates that pre-compound fraction F_{PCN} sensitively depends on the excitation energy per surface nucleon $(E^*/A^{2/3})$ of the composite systems, mass number of the target nuclei. Moreover, as the excitation energy per surface nucleon $(E^*/A^{2/3})$ increases, the pre-compound contribution also increases in a systematic way and then tends to a saturation point. The presently developed systematics may be used to predict the PCN contribution more precisely and can also be used as a new constraint for the further development of theoretical models which describe the PCN process.

The authors are thankful to the Director, VECC, Kolkata, India for extending all the facilities for carrying out the experiments. One of the authors (MKS) thanks the Council of Scientific and Industrial Research (CSIR), New Delhi (Project No. 03(361)16/EMR-11 for its financial support.

References

1. B.P. Singh, H.D. Bhardwaj, R. Prasad, Can. J. Phys. **69**, 1376 (1991).
2. B.P. Singh, M.G.V. Sankaracharyulu, M.A. Ansari, H.D. Bhardwaj, R. Prasad, Int. J. Mod. Phys. E **4**, 823 (1992).
3. M. Avrigeanu, V. Avrigeanu, P. Bem, U. Fischer, M. Honusek, K. Katovsky, C. Manailescu, J. Mrazek, E. Simeckova, L. Zavorka, Phys. Rev. C **89**, 044613 (2014).
4. K. Kim, G.N. Kim, H. Naik, M. Zaman, S.-C. Yang, T.-Y. Song, R. Guin, S.K. Das, Nucl. Phys. A **935**, 65 (2015).
5. M.K. Sharma, H.D. Bhardwaj, Unnati, P.P. Singh, B.P. Singh, R. Prasad, Eur. Phys. J. A **31**, 43 (2007).
6. B.P. Singh, Manoj K. Sharma, M.M. Muthafa, H.D. Bhardwaj, R. Prasad, B.P. Singh, M.K. Sharma, M.M. Musthafa, H.D. Bhardwaj, R. Prasad, Nucl. Instrum. Methods A **562**, 717 (2006).
7. J. Pal, C.C. Dey, P. Banerjee, S. Bose, B.K. Sinha, M.B. Chatterjee, Phys. Rev. C **71**, 034605 (2005).
8. S. Mukherjee, N.L. Singh, G. Kiran Kumar, L. Chaturvedi, Phys. Rev. C **72**, 014609 (2005).
9. L. Westerberg, D.G. Saranties, D.C. Hensley, R.A. Dayras, M.L. Halbert, J.H. Barker, Phys. Rev. C **18**, 796 (1978).
10. D.G. Saranties, L. Westerberg, M.L. Halbert, R.A. Dayras, D.C. Hensley, J.H. Barker, Phys. Rev. C **18**, 774 (1978).
11. D.G. Saranties, L. Westerberg, M.L. Halbert, R.A. Dayras, D.C. Hensley, J.H. Barker, Phys. Rev. C **17**, 601 (1978).
12. J.R. Wu, C.C. Chang, H.D. Holmgren, Phys. Rev. C **19**, 669 (1979).
13. T.C. Awes, G. Poggi, C.K. Gelbke, B.B. Back, B.G. Glagola, H. Breuer, V.E. Ciola, Phys. Rev. C **24**, 89 (1981).
14. M.K. Sharma, P.P. Singh, V. Sharma, M. Shuaib, D.P. Singh, A. Yadav, Unnati, R. Kumar, B.P. Singh, R. Prasad, Phys. Rev. C **96**, 044617 (2016).
15. M.K. Sharma, P.P. Singh, D.P. Singh, A. Yadav, V. Sharma, I. Bala, R. Kumar, A. Yadav, B.P. Singh, R. Prasad, Phys. Rev. C **91**, 014603 (2015).
16. E. Gadioli, E. Gadiolli-Ebra, J.J. Hogan, B.V. Jacab, Phys. Rev. C **29**, 76 (1984).
17. J. Ernst, W. Friedland, H. Stockhorst, Z. Phys. A **328**, 333 (1987).
18. J. Ernst, W. Friedland, H. Stockhorst, Z. Phys. A **308**, 301 (1982).
19. S. Sudar, S.M. Qaim, Phys. Rev. C **73**, 034613 (2006).
20. B.P. Singh, M.G.V. Sankaracharyulu, M.A. Ansari, H.D. Bhardwaj, R. Prasad, Phys. Rev. C **47**, 2055 (1993).
21. X. Peng, F. He, X. Long, Nucl. Instrum. Methods Phys. Res. B **152**, 432 (1999).
22. S. Sudar, S.M. Qaim, Phys. Rev. C **50**, 2408 (1994).
23. K.F. Hassan, S.M. Qaim, Z.A. Saleh, H.H. Coenen, Appl. Radiat. Isot. **64**, 101 (2006).
24. M.S. Uddin, A. Hermanne, S. Sudar, M.N. Aslam, B. Scholten, H.H. Coenen, S.M. Qaim, Appl. Radiat. Isot. **69**, 699 (2011).
25. W.W. Bowman, M. Blann, Nucl. Phys. A **131**, 513 (1969).
26. B.P. Singh, H.D. Bhardwaj, R. Prasad, Nuovo Cimento A **104**, 45 (1991).
27. F. Tarkanyi, F. Ditroi, A. Hermanne, S. Takecs, A.V. Ignatyuk, J. Radioanal. Nucl. Chem. **298**, 277 (2013).
28. P. Mohr, Eur. Phys. J. A **51**, 56 (2015).
29. M. Yigit, M.E. Korkmaz, Mod. Phys. Lett. **33**, 1850155 (2018).
30. D. Suchiang, J. Joseph, B.M. Jyrwa, Indian J. Pure Appl. Phys. **51**, 696 (2013).
31. A.V. Mohan, S.N. Chintalapudi, J. Phys. Soc. Jpn. **63**, 84 (1994).
32. F. Tarkanyi, S. Takacs, B. Kiraly, F. Szelecsenyi, L. Ando, J. Bergman, S.-J. Heselius, O. Solin, A. Hermanne, Yu.N. Shubin, A.V. Ignatyuk, Appl. Radiat. Isot. **67**, 1001 (2009).
33. M.S. Uddin, A. Hermanne, S. Sudar, M.N. Aslam, B. Scholten, H.H. Coenen, S.M. Qaim, Appl. Radiat. Isot. **69**, 699 (2010).
34. M. Ismail, Phys. Rev. C **41**, 87 (1990).
35. M. Furuawa, Nucl. Phys. A **77**, 567 (1966).
36. S. Mukherjee, B.B. Kumar, M.H. Rashid, S.N. Chintalapudi, Phys. Rev. C **55**, 2556 (1997).
37. M. Ismail, Pramana J. Phys. **50**, 173 (1998).
38. N.E. Scott, J.W. Cobble, P.J. Daly, Nucl. Phys. A **119**, 131 (1968).
39. H.E. Kurz, E.W. Jasper, K. Fisscher, F. Hermes, Nucl. Phys. A **168**, 129 (1971).

40. N.P.M. Sathik, M. Afzal Ansari, B.P. Singh, M. Ismail, M.H. Rashid, Phys. Rev. C **66**, 014602 (2002).
41. EXFOR: Experimental Nuclear Reactions, `https://wwww-nds.iaea.org/exfor`.
42. A. Gavron, Phys. Rev. C **21**, 230 (1980).
43. M. Blann, Report PSR-146, NEA Data Bank, Gif-sur-Yvette, France (1991).
44. R. Bass, Nucl. Phys. A **231**, 45 (1974).
45. V.F. Weisskopf, D.H. Ewing, Phys. Rev. **57**, 472 (1940).
46. M. Blann, Phys. Rev. Lett. **28**, 757 (1972).
47. `http://www.srim.org`.
48. E. Browne, R.B. Firestone, *Table of Radioactive Isotopes* (Wiley, New York, 1986).
49. P.M. Endt, At. Data Nucl. Data Tables **26**, 47 (1981).
50. S.K. Kataria, V.S. Ramamurthy, S.K. Kapoor, Phys. Rev. C **18**, 549 (1978).
51. W.D. Myers, W.J. Swiatecki, Ark. Phys. **36**, 343 (1967).
52. F.D. Becchetti, G.W. Greenlees, Phys. Rev. **182**, 1190 (1969).
53. K. Kikuchi, M. Kawai, *Nuclear Matter and Nuclear Reactions* (North Holland Publ. Co., 1968).
54. M. Blann, Nucl. Phys. A **213**, 570 (1973).
55. J.R. Huizenga, L.G. Moretto, Ann. Rev. Nucl. Sci. **22**, 427 (1972).
56. W. Dilg, W. Schantl, H. Vonach, Nucl. Phys. A **217**, 269 (1973).